Probing the energy flow in Bessel light beams using atomic photoionization

A. Surzhykov,[1,2] D. Seipt,[3,4] and S. Fritzsche[3,4]
[1]*Physikalisch-Technische Bundesanstalt, D-38116 Braunschweig, Germany*
[2]*Technische Universität Braunschweig, D-38106 Braunschweig, Germany*
[3]*Helmholtz-Institut Jena, D-07743 Jena, Germany*
[4]*Theoretisch-Physikalisches Institut, Friedrich-Schiller-Universität Jena, D-07743 Jena, Germany*
(Received 22 May 2016; published 27 September 2016)

The growing interest in twisted light beams also requires a better understanding of their complex internal structure. Particular attention is currently being given to the energy circulation in these beams as usually described by the Poynting vector field. In the present study we propose to use the photoionization of alkali-metal atoms as a probe process to measure (and visualize) the energy flow in twisted light fields. Such measurements are possible since the angular distribution of photoelectrons, emitted from a small atomic target, appears sensitive to and is determined by the local direction of the Poynting vector. To illustrate the feasibility of the proposed method, detailed calculations were performed for the ionization of sodium atoms by nondiffractive Bessel beams.

DOI: 10.1103/PhysRevA.94.033420

I. INTRODUCTION

Light beams with a helical phase front, that also carry orbital angular momentum (OAM), have been in the focus of research since the seminal work by Allen *et al.* in 1992 [1]. Today, such *twisted* beams are routinely produced across the electromagnetic spectrum, with photon energies ranging from meV to hundreds of eV, and with the OAM projection on their propagation direction as high as $\hbar m_l \gtrsim 1000\hbar$ [2–4]. The twisted light provides a unique tool for manipulating microparticles [5–7], for multiplexing in optical communications [8,9], or for studying the angular momentum transfer to liquid crystals, Bose-Einstein condensates, or even the bulk of semiconductors [10–12]. During recent years, moreover, intense studies have been performed to explore how to produce high-energy OAM beams by means of high-order-harmonic generation [13] or Compton backscattering [14], and how the OAM of incident light may influence the selection rules in atomic transitions [15–18].

In contrast to the "usual" plane-wave radiation, twisted light typically has a much more complex internal structure. In particular, its intensity distribution in the beam cross section is not uniform but usually appears as concentric (and alternating) dark and bright rings. Also the direction of the energy flow varies significantly within the wave front, and this indicates that the propagation of twisted light is accompanied by internal energy redistribution [19]. Recent studies have revealed, for instance, the possibility of the "negative propagation" of twisted light, i.e., of the backward energy flow in some regions of a beam [20].

The investigation of the energy flow patterns in OAM light beams attracts currently much attention in both experiment and theory [19–21]. It provides valuable information about the "internal structure" of twisted radiation and, in particular, about its spatial and polarization degrees of freedom. The knowledge and control of energy flows is essential, moreover, for various applications such as optical micromanipulation or the development of novel quantum information protocols.

Despite the growing interest in the circulation of the energy in OAM beams, experimental observation of the flow patterns still remains a rather difficult problem. Most of the methods to measure the energy flow are based on either (i) the mechanical action of the optical field upon the probe microparticles or (ii) observations of the intensity profile of the free-space propagating beams [19]. In the present work we propose an alternative and very promising approach that enables one to "visualize" the energy flow fields of twisted beams. This approach employs the fundamental process of the photoionization of alkali-metal atoms by incident (twisted) radiation. Based on detailed theoretical analysis of nondiffractive Bessel light, we show below that the angular distribution of photoelectrons emitted from (small) atomic targets is *uniquely* defined by the direction of the local energy flow. The proposed measurement is likely to become feasible in the near future and may provide valuable information about the energy circulation in twisted light beams.

To describe the ionization of atomic targets by OAM beams, we first recall in the next section the definition of the Bessel waves in terms of their vector potential. By making use of this potential, we derive then the Poynting vector of the twisted (Bessel) radiation and discuss its complex spatial structure. The angular distribution of photoelectrons emitted from a single atom is derived in Sec. III A. A more realistic scenario of a mesoscopic atomic target is discussed later in Sec. III B. Finally, conclusions and a brief outlook of the present work are given in Sec. IV. The relativistic Gaussian units with $\hbar = c = 1$ are used throughout the paper unless stated otherwise.

II. PROPERTIES OF BESSEL LIGHT BEAMS

A. Vector potential

To perform a theoretical analysis of atomic photoionization, one needs to consider also the quantum state of the incident light. In the present study we assume that incoming radiation is *prepared* in the pure Bessel state $|\varkappa\, m\, k_z\, \lambda\rangle$. The Bessel light beam is characterized by a well-defined projection m of the total angular momentum (TAM) upon its propagation direction, chosen as the z axis. Moreover, the longitudinal momentum k_z and the absolute value of the transverse momentum $\varkappa = k_\perp \equiv |\boldsymbol{k}_\perp|$ of the twisted wave (tw) are also kept fixed. The vector potential of such a *nonparaxial* Bessel beam,

$$\mathbf{A}^{(\mathrm{tw})}_{\varkappa m k_z \lambda}(\boldsymbol{r}) = \int \boldsymbol{e}_{\boldsymbol{k}\lambda}\, e^{i\boldsymbol{k}\cdot\boldsymbol{r}}\, a_{\varkappa m}(\boldsymbol{k}_\perp)\, \frac{k_\perp\, dk_\perp\, d\phi_k}{(2\pi)^2}, \tag{1}$$

can be written as a coherent superposition of plane waves $\boldsymbol{e}_{\boldsymbol{k}\lambda}\exp(i\boldsymbol{k}\cdot\boldsymbol{r})$ with wave vectors $\boldsymbol{k} = (k\sin\theta_k\cos\phi_k, k\sin\theta_k\sin\phi_k, k\cos\theta_k)$, energy $\omega = |\boldsymbol{k}|$, and polarization vectors

$$\boldsymbol{e}_{\boldsymbol{k}\lambda} = \sum_{m_s=-1}^{+1} c_{m_s}\, e^{-im_s\phi_k}\, \boldsymbol{\eta}_{m_s}, \tag{2}$$

with the coefficients

$$c_{\pm 1} = \frac{1}{2}(1 \pm \lambda\cos\theta_k), \quad c_0 = \frac{\lambda}{\sqrt{2}}\sin\theta_k. \tag{3}$$

Here, $\theta_k = \arctan(\varkappa/k_z)$ is often called the *opening* angle and $\boldsymbol{\eta}_{0,\pm 1}$ are spherical unit vectors [22]. In Eq. (1) each plane wave is weighted with the amplitude

$$a_{\varkappa m}(\boldsymbol{k}_\perp) = (-i)^m\, e^{im\phi_k}\sqrt{\frac{2\pi}{k_\perp}}\,\delta(k_\perp - \varkappa), \tag{4}$$

with ϕ_k being the azimuthal angle of the wave vector $\boldsymbol{k}$. We assume, moreover, that the plane-wave components are prepared in a pure circularly polarized state that is characterized by the helicity $\lambda = \pm 1$. In classical electrodynamics, the helicity $\lambda = +1$ ($\lambda = -1$) corresponds to electromagnetic radiation with right (left) rotation of the electric field vector.

The *integral* representation (1) of the vector potential $\mathbf{A}^{(\mathrm{tw})}_{\varkappa m k_z \lambda}(\boldsymbol{r})$ is very convenient for the calculation of probabilities of atomic photoexcitation and photoionization (see, e.g., Refs. [15–17,23]). Moreover, it can be easily used to evaluate the observable properties of twisted light. In the next section, for example, we briefly discuss the components of the electromagnetic field as well as the Poynting vector of the Bessel beam.

B. Field components and energy flow

We are ready now to discuss the observable properties of the nonparaxial Bessel light and start from the electromagnetic-field components. For further analysis it is convenient to represent these components in *cylindrical* coordinates with the z axis chosen along the beam propagation direction. By using Eqs. (1) and performing some algebra we can derive, for example, the magnetic field $\boldsymbol{B}^{(\mathrm{tw})} = \boldsymbol{\nabla}\times\boldsymbol{A}^{(\mathrm{tw})}$ as

$$\mathbf{B}^{(\mathrm{tw})} = \boldsymbol{e}_z B_z(\boldsymbol{r}) + \boldsymbol{e}_{r_\perp} B_{r_\perp}(\boldsymbol{r}) + \boldsymbol{e}_{\varphi_r} B_{\varphi_r}(\boldsymbol{r}), \tag{5}$$

where

$$\begin{aligned}
B_z(\boldsymbol{r}) &= \omega\sqrt{\frac{\varkappa}{2\pi}}\, e^{ik_z z}\, e^{im\varphi_r}\, J_m(k_\perp r_\perp)\,\sin\theta_k,\\
B_{r_\perp}(\boldsymbol{r}) &= i\omega\lambda\sqrt{\frac{\varkappa}{2\pi}}\, e^{ik_z z}\, e^{im\varphi_r}\\
&\quad\times(J_{m+1}(k_\perp r_\perp)\,c_{-1} + J_{m-1}(k_\perp r_\perp)\,c_1),\\
B_{\varphi_r}(\boldsymbol{r}) &= \omega\lambda\sqrt{\frac{\varkappa}{2\pi}}\, e^{ik_z z}\, e^{im\varphi_r}\\
&\quad\times(J_{m+1}(k_\perp r_\perp)\,c_{-1} - J_{m-1}(k_\perp r_\perp)\,c_1)
\end{aligned} \tag{6}$$

(see Refs. [15,23] for further details). In these expressions, $\boldsymbol{r} = (r_\perp, \varphi_r, z)$, J_m are the Bessel functions of the first kind, and the coefficients c_{m_s} are given by Eq. (3). The electric field components can be easily obtained from these expressions by noting that $\boldsymbol{E}^{(\mathrm{tw})} = i\lambda\boldsymbol{B}^{(\mathrm{tw})}$ (see, e.g., Ref. [15]). As usual, the *physical* fields are the real parts of $\boldsymbol{E}^{(\mathrm{tw})}$ and $\boldsymbol{B}^{(\mathrm{tw})}$.

The electric and magnetic fields from above can be used to derive finally the time-averaged Poynting vector $\boldsymbol{P}^{(\mathrm{tw})} = \mathrm{Re}(\boldsymbol{E}^{(\mathrm{tw})}\times\boldsymbol{B}^{(\mathrm{tw})*})/2$. This vector characterizes both the intensity profile and the energy flow of the light, and reads in cylindrical coordinates as

$$\boldsymbol{P}^{(\mathrm{tw})}(\boldsymbol{r}) = \boldsymbol{e}_{r_\perp} P_{r_\perp}(\boldsymbol{r}) + \boldsymbol{e}_{\varphi_r} P_{\varphi_r}(\boldsymbol{r}) + \boldsymbol{e}_z P_z(\boldsymbol{r}), \tag{7}$$

where

$$\begin{aligned}
P_{r_\perp}(\boldsymbol{r}) &= 0,\\
P_{\varphi_r}(\boldsymbol{r}) &= \frac{\varkappa\omega^2}{4\pi}\,\sin\theta_k\, J_m(k_\perp r_\perp)\\
&\quad\times(J_{m+1}(k_\perp r_\perp)\,c_{-1} + J_{m-1}(k_\perp r_\perp)\,c_{+1}),\\
P_z(\boldsymbol{r}) &= \frac{\varkappa\omega^2\lambda}{4\pi}\left(J^2_{m-1}(k_\perp r_\perp)\,c^2_{+1} - J^2_{m+1}(k_\perp r_\perp)\,c^2_{-1}\right).
\end{aligned} \tag{8}$$

As seen from these expressions, the radial component of the Poynting vector vanishes identically, $P_{r_\perp} = 0$, thus making explicit that the Bessel beams are nondiffractive as known from the literature. Moreover, the other two components, P_{φ_r} and P_z, depend only on the transverse coordinate $r_\perp$ but *not* on the angle φ_r. This implies that spatial properties of the (time-averaged) Bessel light possess azimuthal symmetry. For example, the intensity profile of the beam in the plane normal to its propagation direction (z axis) is given by

$$I_\perp(r_\perp) = |P_z(\boldsymbol{r})| \tag{9}$$

and exhibits the concentric ring pattern with a central zero-intensity spot; see Fig. 1. Similarly, also the (local) direction of the energy flow in the Bessel beam does not depend on the azimuthal angle φ_r but is characterized by the polar tilt angle:

$$\theta_P(r_\perp) = \arctan\frac{P_{\varphi_r}}{P_z}, \tag{10}$$

which is defined with respect to the propagation z axis. As seen from the bottom panel of Fig. 1, the angle θ_P strongly depends on the distance $r_\perp$ from the center of the Bessel beam. While this angle is rather small near the "rings" of high intensity and with a predominant energy flow in the forward (z) direction, it becomes large, $|\theta_P| \gtrsim 60^\circ$, in the low-intensity regions, and where the energy flow is almost perpendicular to the beam propagation axis. Such a complex structure of twisted Bessel beams obviously affects also all atomic photoexcitation and photoionization processes. Therefore, an analysis of the properties of excited atoms or ionized electrons may reveal information about the spatial structure of Bessel radiation.

III. ANGULAR DISTRIBUTIONS OF PHOTOELECTRONS

A. Photoionization of a single atom

We start the analysis of atomic ionization by Bessel light from the simplest possible target that consists of just a *single* atom. Both the probability of ionization of this atom and the

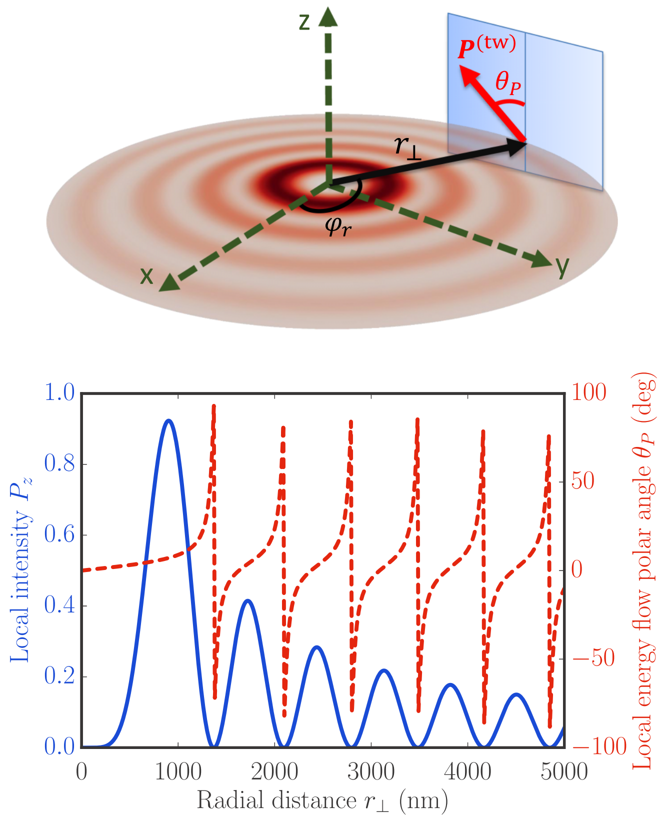

FIG. 1. Top: The intensity profile of the Bessel beam in the xy plane, perpendicular to its propagation direction (z axis), exhibits concentric right structure. The direction of the Poynting vector (7) with respect to the z axis is characterized by the tilt angle θ_P which depends solely on the transverse distance $r_\perp$ from the center of the beam. Bottom: The transverse intensity $I_\perp(r_\perp)$ (blue solid line) and the tilt angle $\theta_P(r_\perp)$ of the Poynting vector (red dashed line) of twisted light with energy $\hbar\omega = 5$ eV, helicity $\lambda = +1$ (i.e., right circular polarization), TAM projection $m = 4$, and opening angle $\theta_k = 10°$.

properties of emitted photoelectrons can be expressed in terms of the (square of the) matrix element:

$$M_{fi}^{(\mathrm{tw})}(\boldsymbol{b}) = \int \psi_f^*(\boldsymbol{r})\, \mathbf{A}_{\varkappa m k_z \lambda}^{(\mathrm{tw})}(\boldsymbol{r}+\boldsymbol{b})\, \hat{\boldsymbol{p}}\, \psi_i(\boldsymbol{r})\, d\boldsymbol{r}. \tag{11}$$

In this expression, written in the nonrelativistic framework, $\psi_i(\boldsymbol{r})$ and $\psi_f(\boldsymbol{r})$ are Schrödinger wave functions of the initial-bound and final-continuum electrons, respectively, while $\hat{\boldsymbol{p}}$ is the electron linear momentum operator, and the vector potential of incident light is given by Eq. (1). We note that the light vector potential $\mathbf{A}_{\varkappa m k_z \lambda}^{(\mathrm{tw})}(\boldsymbol{r}+\boldsymbol{b})$ needs to be taken at the position $\boldsymbol{b}$ of the target atom within the Bessel wave front. This so-called impact parameter (vector) $\boldsymbol{b}$ is always normal to the propagation direction of the beam, and $b = 0$ refers to an atom at the beam center with zero intensity.

The matrix element (11) can be readily employed to study photoionization of low-Z hydrogenlike ions and—within the single-active-electron approach—of light alkali-metal atoms. If the photon energy is not too high, the photoionization is well described by the leading electric-dipole ($E1$) transition. In this approximation, we can further simplify the $M_{fi}^{(\mathrm{tw})}$ by taking $e^{i\boldsymbol{k}\cdot\boldsymbol{r}} \approx 1$ in the integral representation (1) of the vector potential:

$$M_{fi}^{(\mathrm{tw},E1)}(\boldsymbol{b}) = \mathbf{A}_{\varkappa m k_z \lambda}^{(\mathrm{tw})}(\boldsymbol{b}) \cdot \boldsymbol{d}_{if}. \tag{12}$$

This $E1$ approach also implies that the matrix element for the atomic ionization by twisted Bessel light factorizes into the product of (i) the light vector potential at the *location* of a target atom and (ii) the standard dipole matrix element

$$\boldsymbol{d}_{if} = \int \psi_f^*(\boldsymbol{r})\, \hat{\boldsymbol{p}}\, \psi_i(\boldsymbol{r})\, d\boldsymbol{r}, \tag{13}$$

whose evaluation is well established (see, e.g., Ref. [24]).

Using the dipole matrix element (12) we are ready now to derive the angular distribution W_b^{single} of an electron ionized by the twisted Bessel light. In practice, the explicit form of this distribution depends on the setup under which the electron emission is observed. In the present work, we propose to "detect" the photoelectron in a plane, normal to the impact parameter vector $\boldsymbol{b}$ and which, as seen from Eqs. (8) and Fig. 1, coincides with the plane of the Poynting vector of incident light. We therefore expect the electron emission pattern to be sensitive to the (direction of) $\boldsymbol{P}^{(\mathrm{tw})}(\boldsymbol{r})$ at $\boldsymbol{r} = \boldsymbol{b}$. Indeed, inserting the vector potential (1) into Eq. (12), requesting $\boldsymbol{b}\cdot\boldsymbol{p} = 0$, and performing some simple algebra, we find

$$W_b^{\mathrm{single}}(\theta) = \mathcal{N} \sin^2(\theta - \theta_P(b)), \tag{14}$$

where $\mathcal{N}$ is a normalization constant and where both the tilt angle of the Poynting vector $\theta_P(b)$ and the electron emission angle θ are defined with respect to the beam propagation (z) axis. Equation (14) clearly shows that the angular distribution of a photoelectron, if ionized at a distance $r_\perp = b$ from the center of the Bessel beam, depends upon the *direction* of the Poynting vector $\boldsymbol{P}^{(\mathrm{tw})}(\boldsymbol{b})$ at the location of the target. That is, electron emission is forbidden in parallel or antiparallel to $\boldsymbol{P}^{(\mathrm{tw})}$, while W_b^{single} is maximal for $\theta = \theta_P(b) + 90°$.

The dependence of $W_b^{\mathrm{single}}(\theta)$ upon the impact parameter b and the tilt $\theta_P(b)$ of the Poynting vector is displayed in Fig. 2. This figure shows that near the center of the wave front the Poynting vector is parallel to the beam propagation direction (z axis) and, hence, the photoelectron is emitted predominantly under the angle $\theta = 90°$. In contrast, if the $\boldsymbol{P}^{(\mathrm{tw})}$ is (almost) normal to the beam propagation, as in the first low-intensity ring, the electron angular distribution is maximal at forward and backward angles with respect to the z axis. This sensitivity of the electron emission pattern to the direction of the energy flow is well known for the atomic ionization by plane-wave light [24,25]. In that case and in the dipole approximation, the electron emission pattern also has a characteristic $\sin^2\theta$ shape, where θ is defined with respect to the wave vector of incident light. In contrast to the twisted beams, however, the direction of the plane-wave Poynting vector $\boldsymbol{P}^{(\mathrm{pl})}$ is constant over the entire wave front and, hence, the photoelectron angular distribution does not change with the position of a target atom.

B. Photoionization of a mesoscopic atomic target

Equation (14) shows that the angular distribution of the emitted electrons can be utilized for studying the energy flow, i.e., the Poynting vector field in Bessel light beams.

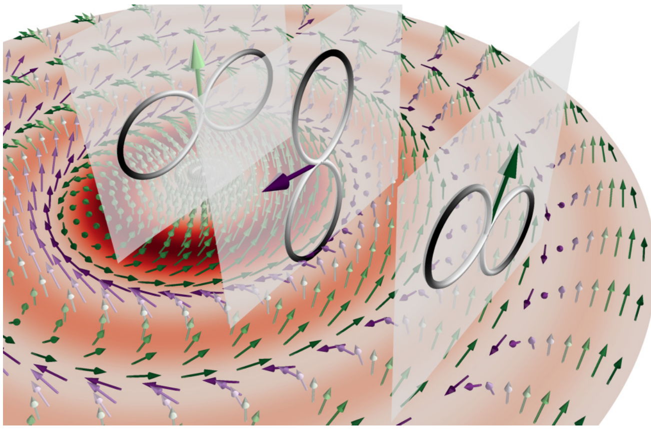

FIG. 2. The intensity profile and the Poynting vector (field) of the Bessel light beam. In addition, we here also display the angular distributions of an electron (gray line) ionized at three different distances from the center of the beam. Obviously, these angular distributions, if measured in the plane normal to the impact parameter vector $\boldsymbol{b}$, are uniquely defined by the direction of the Poynting vector $\boldsymbol{P}^{(\rm tw)}(\boldsymbol{b})$. Calculations have been performed for sodium target atoms and for the same set of beam parameters as used in Fig. 1.

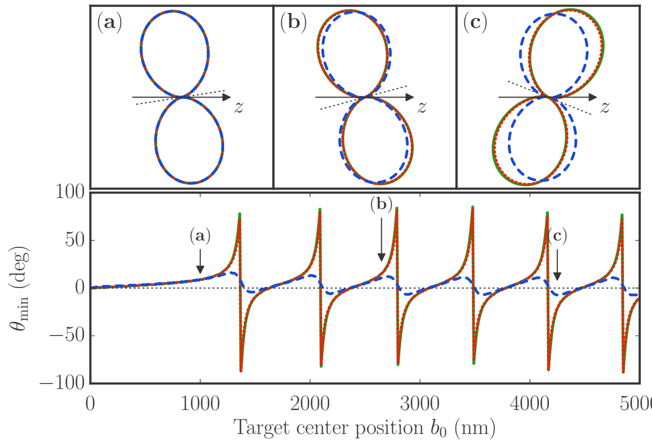

FIG. 3. Top: The angular distribution of electrons photoionized from sodium atomic targets located at distances (a) 1000 nm, (b) 2650 nm, and (c) 4250 nm from the beam center. Bottom: The angle $\theta_{\rm min}$ at which the photoelectron angular distribution is minimal. The calculations for both panels have been performed for the single-atom target (green solid line) as well as for mesoscopic targets of size $\sigma =$ 20 nm (red dotted line) and 100 nm (blue dashed line). Parameters of the incident Bessel beam are the same as used in Fig. 1.

This expression for $W_b^{\rm single}(\theta)$ has been derived for just a single target atom, placed at some well-defined position. In fact, the experiments with single alkali-metal-like atoms (and ions), localized with nanometer precision and interacting with tailored light beams, are feasible today [26,27]. These experiments make use of a laser-cooled atom trapped in a microstructured Paul trap. However, the successful realization of the proposed photoionization measurement with a single-atom target can be hampered by statistical issues. Below, therefore, we discuss a more realistic scenario in which the twisted Bessel light interacts with a mesoscopic atomic target. The atomic density of this target in the plane of the incident wave front (xy plane; see Fig. 1) is assumed to follow the Gaussian distribution

$$f(\boldsymbol{b}) = \frac{1}{2\pi\sigma^2}\, e^{-\frac{(\boldsymbol{b}-\boldsymbol{b}_0)^2}{2\sigma^2}}. \tag{15}$$

In this formula, σ is the width of the target and the vector $\boldsymbol{b}_0$ points from the vortex line of the twisted beam to the center of the target (cloud). Making use of Eq. (15) and the transition matrix element (11), we can compute the angular distribution of electrons ionized from a mesoscopic target:

$$W_{\sigma,b_0}^{\rm target}(\theta) = C \int f(\boldsymbol{b}) \left| M_{fi}^{(\rm tw)}(\boldsymbol{b}) \right|^2 \frac{d^2\boldsymbol{b}}{(2\pi)^2}. \tag{16}$$

This expression is general and accounts for the size and position of a target as well as for the non-electric-dipole effects in the electron-photon interaction. Its further evaluation is rather lengthy and is not shown in detail for the sake of brevity.

We can directly apply Eq. (16) to investigate (i) how the size of the atomic target σ affects the angular distribution of the photoelectrons and (ii) to which extent measurements of $W_{\sigma,b_0}^{\rm target}(\theta)$ provide information about the Poynting vector of light. In Fig. 3, for example, we present numerical results as obtained from Eq. (16) and with the help of the RATIP computer code [28] for two clouds of sodium atoms with size $\sigma = 20$ nm (red dotted line) and 100 nm (blue dashed line). These results are compared with the prediction of Eq. (14) for a single Na atom, located at the center of the cloud $\boldsymbol{b} = \boldsymbol{b}_0$ (red solid line). Again, calculations have been performed for the incident twisted light with energy 5 eV, opening angle $\theta_k = 10^\circ$, right circular polarization of the plane-wave components ($\lambda = +1$), and the projection of the total angular momentum $m = 4$. Moreover, the target atoms were assumed to be in the $1s^2\, 2s^2\, 2p^6\, 3s$ ground state before the ionization.

As seen from the top panel of Fig. 3, the angular distribution of electrons coincides for relatively small targets with $\sigma \lesssim$ 20 nm almost completely with that of a single atom, $W_b^{\rm single}(\theta)$. However, significant deviations from the $\sin^2(\theta - \theta_P(b))$ shape can occur as the size of the target increases. For a target of size $\sigma = 100$ nm and centered at position $b = 4250$ nm, for example, the $W_{\sigma,b_0}^{\rm target}(\theta)$ tilts by almost 15° with respect to $W_b^{\rm single}(\theta)$. Moreover, in contrast to Eq. (14), the minimum value of the angular distribution is not *zero*, although it is still rather small. This behavior follows from the fact that the electron can be ionized at some distant spots of the (large) target at which the directions of the Poynting vector may differ significantly. In this case one observes the superposition of the angular distributions (14) for rather different angles $\theta_P(b)$ and with different weights $\mathcal{N}$.

It also follows from Eq. (14) that the *minimum* (zero) of the photoelectron emission pattern $W_b^{\rm single}(\theta)$ always marks the direction of the Poynting vector $\boldsymbol{P}^{\rm tw}(\boldsymbol{b})$ at a particular impact parameter $r_\perp = b$ within the wave front. Therefore, since $W_{\sigma,b_0}^{\rm target}(\theta) \approx W_b^{\rm single}(\theta)$ for sufficiently small targets, the angular distribution of electrons emitted from such clouds can also be employed to image the energy flow in the Bessel beams. In the bottom panel of Fig. 3, for example, we display the angle $\theta_{\rm min}^{\rm target}$ under which the electron emission $W_{\sigma,b}^{\rm target}(\theta)$ is minimal and compare it with that of the Poynting vector θ_P (solid green line). Similar as before, calculations have been performed for different positions b_0 and sizes σ of the atomic sodium target. As seen from the figure, the $\theta_{\min}^{\text{target}}$ is virtually identical to the tilt angle of the Poynting vector for the targets with width $\sigma \lesssim 20$ nm. However, the minimum-emission angle $\theta_{\min}^{\text{target}}$ may significantly deviate from the θ_P if the target size σ exceeds 100 nm. Indeed, the discrepancy becomes most pronounced for impact parameters b_0 for which the intensity of the Bessel radiation is low and energy flows (almost) normally to the beam propagation direction; see Figs. 1 and 3.

IV. SUMMARY AND OUTLOOK

In summary, we have investigated the ionization of an alkali-metal atom by twisted Bessel light. Special attention was paid to the angular distribution of an emitted photoelectron. We found that the electron emission pattern depends on the position of a target atom within the light wave front and that it is *uniquely* defined by the direction of the Poynting vector of the incident radiation at that position. The sensitivity of the photoelectron angular distribution to the (direction of the) Poynting vector persists also for the ionization of mesoscopic atomic ensembles whose size, however, should not exceed ~50 nm. The production of hundred-nanometer-size clouds of alkali-metal atoms has been recently demonstrated experimentally with the help of evaporative cooling [29]. Further development of cooling and trapping techniques will likely make the proposed photoionization experiment feasible in the near future.

For the sake of brevity we restricted the present study to the particular case of incident Bessel light. Of course, the photoionization of alkali-metal atoms can be employed for probing the energy flow in *other* classes of (twisted) light beams, such as, for example, Laguerre-Gaussian modes. The systematic and comprehensive analysis of these photoionization measurements is currently under way and will be presented elsewhere.

[1] L. Allen, M. W. Beijersbergen, R. J. C. Spreeuw, and J. P. Woerdman, Phys. Rev. A **45**, 8185 (1992).
[2] J. He, X. Wang, D. Hu, J. Ye, S. Feng, Q. Kan, and Y. Zhang, Opt. Express **21**, 20230 (2013).
[3] J. Bahrdt, K. Holldack, P. Kuske, R. Müller, M. Scheer, and P. Schmid, Phys. Rev. Lett. **111**, 034801 (2013).
[4] Y. Shen, G. T. Campbell, B. Hage, H. Zou, B. C. Buchler, and P. K. Lam, J. Opt. **15**, 044005 (2013).
[5] H. He, M. E. J. Friese, N. R. Heckenberg, and H. Rubinsztein-Dunlop, Phys. Rev. Lett. **75**, 826 (1995).
[6] N. Simpson, K. Dholakia, L. Allen, and M. Padgett, Opt. Lett. **22**, 52 (1997).
[7] M. Padgett and R. Bowman, Nat. Photonics **5**, 343 (2011).
[8] N. Bozinovic, Y. Yue, Y. Ren, M. Tur, P. Kristensen, H. Huang, A. E. Willner, and S. Ramachandran, Science **340**, 1545 (2013).
[9] J. P. Torres, Nat. Photonics **6**, 420 (2012).
[10] G. Molina-Terriza, J. P. Torres, and L. Torner, Nat. Phys. **3**, 305 (2007).
[11] G. F. Quinteiro and P. I. Tamborenea, Phys. Rev. B **82**, 125207 (2010).
[12] J. P. Torres and L. Torner, *Twisted Photons: Applications of Light with Orbital Angular Momentum* (Wiley-VCH, Weinheim, 2011).
[13] G. Gariepy, J. Leach, K. T. Kim, T. J. Hammond, E. Frumker, R. W. Boyd, and P. B. Corkum, Phys. Rev. Lett. **113**, 153901 (2014).
[14] U. D. Jentschura and V. G. Serbo, Phys. Rev. Lett. **106**, 013001 (2011).
[15] A. Afanasev, C. E. Carlson, and A. Mukherjee, Phys. Rev. A **88**, 033841 (2013).
[16] H. M. Scholz-Marggraf, S. Fritzsche, V. G. Serbo, A. Afanasev, and A. Surzhykov, Phys. Rev. A **90**, 013425 (2014).
[17] A. Afanasev, C. E. Carlson, and A. Mukherjee, J. Opt. Soc. Am. B **31**, 2721 (2014).
[18] J. D. Rodrigues, L. G. Marcassa, and J. T. Mendonça, J. Phys. B **49**, 074007 (2016).
[19] A. Bekshaev, K. Y. Bliokh, and M. Soskin, J. Opt. **13**, 053001 (2011).
[20] A. V. Novitsky and D. V. Novitsky, J. Opt. Soc. Am. A **24**, 2844 (2007).
[21] O. V. Angelsky, A. Ya. Bekshaev, P. P. Maksimyak, A. P. Maksimyak, S. G. Hanson, and C. Yu. Zenkova, Opt. Express **20**, 3563 (2012).
[22] D. A. Varshalovich, A. N. Moskalev, and V. K. Khersonskii, *Quantum Theory of Angular Momentum* (World Scientific, Singapore, 1988).
[23] O. Matula, A. G. Hayrapetyan, V. G. Serbo, A. Surzhykov, and S. Fritzsche, J. Phys. B **46**, 205002 (2013).
[24] B. H. Bransden and C. J. Joachain, *Physics of Atoms and Molecules* (Longman Group, New York, 1983).
[25] J. Eichler and Th. Stöhlker, Phys. Rep. **439**, 1 (2007).
[26] U. Poschinger, A. Walther, K. Singer, and F. Schmidt-Kaler, Phys. Rev. Lett. **105**, 263602 (2010).
[27] C. T. Schmiegelow, J. Schulz, H. Kaufmann, T. Ruster, U. G. Poschinger, and F. Schmidt-Kaler, arXiv:1511.07206.
[28] S. Fritzsche, Comput. Phys. Commun. **183**, 1525 (2012).
[29] R. Bourgain, J. Pellegrino, A. Fuhrmanek, Y. R. P. Sortais, and A. Browaeys, Phys. Rev. A **88**, 023428 (2013).